

which may be treated by statistical mechanics—are typically chaotic. The result also supports the role of dynamical instability in non-equilibrium fluids<sup>12–17,28</sup>. □

Received 29 December 1997; accepted 8 June 1998.

- Eckmann, J.-P., Oliffson Kamphorst, S., Ruelle, D. & Ciliberto, S. Lyapunov exponents from time series. *Phys. Rev. A* **34**, 4971–4979 (1986).
- Roux, J.-C., Simoyi, R. H. & Swinney, H. L. Observation of a strange attractor. *Physica D* **8**, 257–266 (1983).
- Wisdom, J., Peale, S. J. & Mignard, F. The chaotic rotation of Hyperion. *Icarus* **58**, 137–152 (1984).
- Klavetter, J. J. Rotation of Hyperion. I. Observations. *Astron. J.* **97**, 570–579 (1989).
- Laskar, J. A numerical experiment on the chaotic behaviour of the Solar System. *Nature* **338**, 237–238 (1989).
- Eckmann, J.-P. & Ruelle, D. Ergodic theory of chaos and strange attractors. *Rev. Mod. Phys.* **57**, 617–656 (1985).
- Livi, R., Politi, A. & Ruffo, S. Distribution of characteristic exponents in the thermodynamic limit. *J. Phys. A* **19**, 2033–2040 (1986).
- Posch, H. A. & Hoover, W. G. Lyapunov instability of dense Lennard-Jones fluids. *Phys. Rev. A* **38**, 473–482 (1988); Equilibrium and nonequilibrium Lyapunov spectra for dense fluids and solids. *Phys. Rev. A* **39**, 2175–2188 (1989).
- Dellago, Ch., Posch, H. A. & Hoover, W. G. Lyapunov instability in a system of hard disks in equilibrium and nonequilibrium steady states. *Phys. Rev. E* **53**, 1485–1501 (1996).
- Gaspard, P. *Chaos, Scattering Theory, and Statistical Mechanics* (Cambridge Univ. Press, 1998).
- Krylov, N. Relaxation processes in statistical systems. *Nature* **153**, 709–710 (1944).
- Bunimovich, L. A. & Sinai, Ya. G. Statistical properties of Lorentz gas with periodic configuration of scatterers. *Commun. Math. Phys.* **78**, 479–497 (1981).
- Evans, D. J., Cohen, E. G. D. & Morriss, G. P. Viscosity of a simple fluid from its maximal Lyapunov exponents. *Phys. Rev. A* **42**, 5990–5997 (1990).
- Gaspard, P. & Nicolis, G. Transport properties, Lyapunov exponents, and entropy per unit time. *Phys. Rev. Lett.* **65**, 1693–1696 (1990).
- Dorfman, J. R. & Gaspard, P. Chaotic scattering theory of transport and reaction-rate coefficients. *Phys. Rev. E* **51**, 28–35 (1995).
- Ruelle, D. Positivity of entropy production in nonequilibrium statistical mechanics. *J. Stat. Phys.* **85**, 1–23 (1996).
- Chernov, N. I., Eyink, G. L., Lebowitz, J. L. & Sinai, Ya. G. Derivation of Ohm's law in a deterministic mechanical model. *Phys. Rev. Lett.* **70**, 2209–2212 (1993).
- Gallavotti, G. & Cohen, E. G. D. Dynamical ensembles in nonequilibrium statistical mechanics. *Phys. Rev. Lett.* **74**, 2694–2697 (1995); Dynamical ensembles in stationary states. *J. Stat. Phys.* **80**, 931–970 (1995).
- Gaspard, P. Can we observe microscopic chaos in the laboratory? *Adv. Chem. Phys. XCIX*, 369–392 (1997).
- Gaspard, P. & Wang, X.-J. Noise, chaos, and  $(\epsilon, \tau)$ -entropy per unit time. *Phys. Rep.* **235**, 291–345 (1993).
- Chaitin, G. J. *Algorithm Information Theory* (Cambridge Univ. Press, 1987).
- Kolmogorov, A. N. Combinatorial foundations of information theory and the calculus of probabilities. *Russ. Math. Survey* **38**, 29–40 (1983).
- Grassberger, P. & Procaccia, I. Estimation of the Kolmogorov entropy from a chaotic signal. *Phys. Rev. A* **28**, 2591–2593 (1983).
- Cohen, A. & Procaccia, I. Computing the Kolmogorov entropy from time signals of dissipative and conservative dynamical systems. *Phys. Rev. A* **31**, 1872–1882 (1985).
- Ott, E. *Chaos in Dynamical Systems* (Cambridge Univ. Press, 1993).
- Kolmogorov, A. N. On the Shannon theory of information transmission in the case of continuous signals. *IRE Trans. Information Theory IT-2*, 102–108 (1956).
- Berger, T. Information rates of Wiener processes. *IEEE Trans. Information Theory IT-16*, 134–139 (1970).
- Tél, T., Gaspard, P. & Nicolis, G. (eds) *Chaos* **8**, (Focus Issue on Chaos and Irreversibility) (1998).
- van Beijeren, H. Transport properties of stochastic Lorentz models. *Rev. Mod. Phys.* **54**, 195–234 (1982).
- Grier, D. G. & Murray, C. A. in *Structure and Dynamics of Strongly Interacting Colloids and Supramolecular Aggregates in Solution* (eds Chen, S. H., Huang, J. S. & Tartaglia, P.) 145 (NATO ASI Ser. C, 369, Kluwer, Boston, 1991).
- Schaertl, W. & Sillescu, H. Dynamics of colloidal hard spheres in thin aqueous suspension layers. *J. Colloid Interface Sci.* **155**, 313–318 (1993).

**Acknowledgements.** P.G. was supported by the National Fund for Scientific Research (FNRS Belgium); J.R.D. thanks T. Gilbert for helpful remarks, and the US NSF for support; M.E.B. thanks the Physics Department at the University of Utah for support. This work was supported in part by the IUAP/PAI program of the Belgium Government and by the Banque Nationale de Belgique.

Correspondence and requests for materials should be addressed to P.G. (e-mail: gaspard@ulb.ac.be).

## Controlling local disorder in self-assembled monolayers by patterning the topography of their metallic supports

Joanna Aizenberg, Andrew J. Black & George M. Whitesides

Department of Chemistry and Chemical Biology, Harvard University, 12 Oxford Street, Cambridge, Massachusetts 02138, USA

Micropatterning is a powerful method for controlling surface properties, with applications from cell biology to electronics<sup>1–8</sup>. Self-assembled monolayers (SAMs) of alkanethiolates on gold and silver<sup>9–11</sup>—the structures most widely used for preparing organic films with specific surface properties—are usually patterned by

partitioning the surface into regions formed from different thiols<sup>12–15</sup>. Here we describe a way to pattern SAMs using a single alkanethiol on substrates consisting of regions of different topography: planar islands of one metal on the surface of a second (which may be different from or the same as the first). These topographically patterned SAMs consist of three regions: two planar surfaces and a transition region between the two. The characters of the SAMs on these three regions were inferred from images of three structures that form on them: condensation figures, patterns of crystals of CaCO<sub>3</sub> and regions of selective etching. The transition region is more active in the processes generating these structures than either of the two planar regions, and we propose that this activity is due to the relatively high disorder in the organic film there. We believe that this ability to

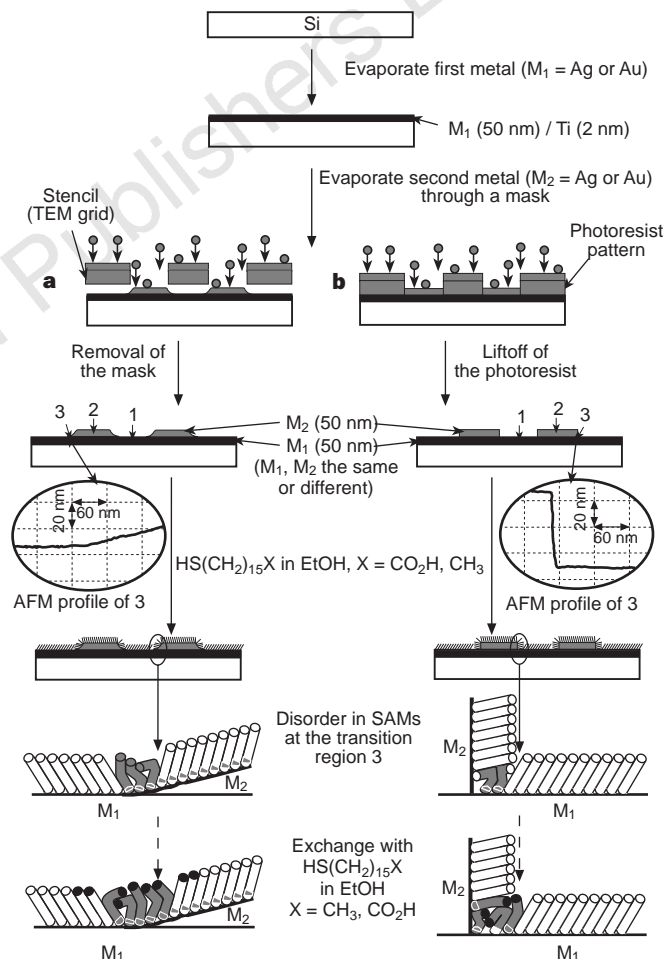


**Figure 1** Schematic representation of the procedures used for fabrication of SAMs supported on topographically patterned metal surfaces. **a**, Patterned deposition of the overlayer of a metal on the surface of another metal (which might be the same or different) through a stencil. **b**, Area-selective deposition of the overlayer of a metal on the surface of another metal protected by a pattern in photoresist, followed by lift-off of the photoresist. The height profiles of the micropatterned surfaces recorded using atomic force microscopy (AFM) show that procedure **b** generates sharper edges for the patterned features than procedure **a**. The details of the surface in the transition region at the level of the grain and domain sizes and boundaries were not studied. The structure of the SAM shown is schematic. In the experiments involving formation of condensation figures, we allowed the thiol in the transition region of the SAM to exchange with a different thiol in solution. To form the patterns, silicon wafers (test grade, n or p type; Silicon Sense, Nashua, NH) were coated with 2.5 nm of Ti to promote adhesion, and then with 50 nm of metal (Ag or Au) using an electron beam evaporator and a stencil mask or patterned photoresist.

**control the local disorder in a SAM with high resolution will be important in controlling processes such as nucleation, wetting, adhesion and etching on scales of below 50 nm to 5  $\mu\text{m}$ .**

In this approach to micropatterning, we fabricate patterned substrates by evaporating one metal (Au or Ag) onto the surface of a second (Au or Ag) through a stencil mask or a patterned photoresist (Fig. 1). We describe these surfaces using the nomenclature  $M_2$ -on- $M_1$ : that is,  $M_2$  (the second metal) evaporated on  $M_1$  (the first). We formed SAMs on these patterned substrates by immersing them in a 10 mM solution of  $\text{HS}(\text{CH}_2)_{15}\text{X}$  ( $\text{X} = \text{CH}_3$  or  $\text{CO}_2\text{H}$ ) in ethanol for 1 h. SAMs of the same alkanethiol formed on different metals differ in structure<sup>9–11</sup>, and we expected, therefore, that the SAM at the border between two different metals would have a distinct and probably less-ordered structure (region 3 in Fig. 1) than the larger planar regions (regions 1 and 2 in Fig. 1). It seemed possible that the region of SAM at sharp steps in the topography of the same metal might also have abnormal structure.

To test the hypothesis that the transition region would be disordered, the topographically patterned substrates supporting one thiolate—either methyl- or acid-terminated—were allowed to soak in a solution of the second (10 mM). We expected the disordered regions of SAMs to be more labile than the ordered regions, and thus to exchange selectively<sup>14–16</sup>. We examined the wettability of the surfaces using condensation figures<sup>17–19</sup> to visualize modifications in the SAM resulting from this exchange (Fig. 2). The best visualization of the transition region was achieved when we used long exchange ( $\sim 10$  h) with the alternative thiol. When a methyl-terminated SAM was allowed to exchange with the acid-terminated thiol, condensation figures on the modified surface consisted of elongated drops of water at a hydrophilic border between the two metals (Fig. 2a–c). When the SAMs were formed in the reverse order—first from the acid-terminated thiol and then

exchanged with methyl-terminated thiol—the pattern of wetting was also reversed: water drops nucleated everywhere except at a hydrophobic border between the metals (Fig. 2d, e). The condensation figures outlining transition regions were particularly pronounced when  $M_1$  was not the same as  $M_2$  (Fig. 2b, c, e). The wetting of surfaces that were not subjected to exchange was largely homogeneous across the surface (Fig. 2a–e), with insignificant preference for nucleation at the boundaries when  $M_1$  was not the same as  $M_2$  presumably due to the pinning of water drops by the local disorder in the SAM. Exchange experiments using substrates prepared by deposition of  $M_2$  at an angle of  $\sim 20^\circ$  from the normal show that the size and shape of the exchanged region—which is related, we presume, to the structure of the disordered SAM—depend on the topology of the boundary between the two metals (Fig. 2c).

These preferential exchange experiments establish that there are three distinct regions in the SAMs supported on micropatterned mixed metal substrates, and suggest that one of these regions is a narrow region of a labile, disordered SAM at the border between the two metals. So this technique provides, to our knowledge, a new concept in patterning surfaces—controlling the local disorder in SAMs on a submicrometre scale by manipulating the topography and composition of the supporting metals. The boundaries between the two metals present disordered regions on the surface, and can be thus used to pattern processes that are sensitive to surface structure. For processes that require the formation of narrow features, the best system is a substrate in which  $M_1$  is the same as  $M_2$ , patterned using a photoresist mask to produce vertical walls in the relief. For processes that do not require the formation of narrow features, a combination of different metals gives a more pronounced effect. We demonstrate two further examples of this method: nucleation of crystal growth, and etching of the underlying metal.

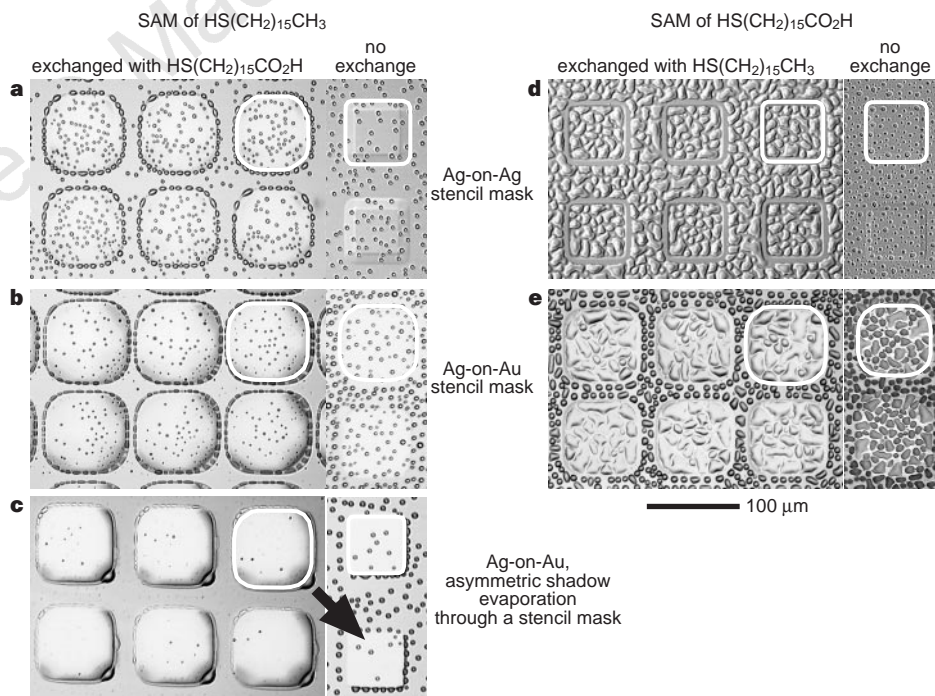


**Figure 2** Optical micrographs of the condensation figures (CFs) formed on SAMs of alkanethiols supported on micropatterned metal substrates. These substrates were fabricated by depositing silver (50 nm) on silver (**a** and **d**), or silver (50 nm) on gold (**b**, **e** and **c**) using a stencil (a TEM grid). The geometries of the islands of the second metal (shown in overlays) depend on the distance between the mask and the substrate and on the angle between the beam and substrate. **a–c**, CFs formed on SAMs of  $\text{HS}(\text{CH}_2)_{15}\text{CH}_3$  exchanged with  $\text{HS}(\text{CH}_2)_{15}\text{CO}_2\text{H}$ ; **d**, **e**, CFs formed on SAMs of  $\text{HS}(\text{CH}_2)_{15}\text{CO}_2\text{H}$  exchanged with  $\text{HS}(\text{CH}_2)_{15}\text{CH}_3$ . The rightmost columns

of each pattern show CFs formed on the control patterned substrates supporting corresponding SAMs that were not subjected to exchange. The surfaces were derivatized initially by exposing them to a solution of one thiol (10 mM in ethanol) for 30 s. The substrates were rinsed with ethanol and allowed to soak in a solution of the second thiol for 10 h. We observed CFs directly by breathing on the samples under an optical microscope. The substrate in **c** was prepared by asymmetric shadow evaporation of Ag through a stencil mask—the direction of the beam (indicated by an arrow) was  $\sim 20^\circ$  from the normal to the surface.

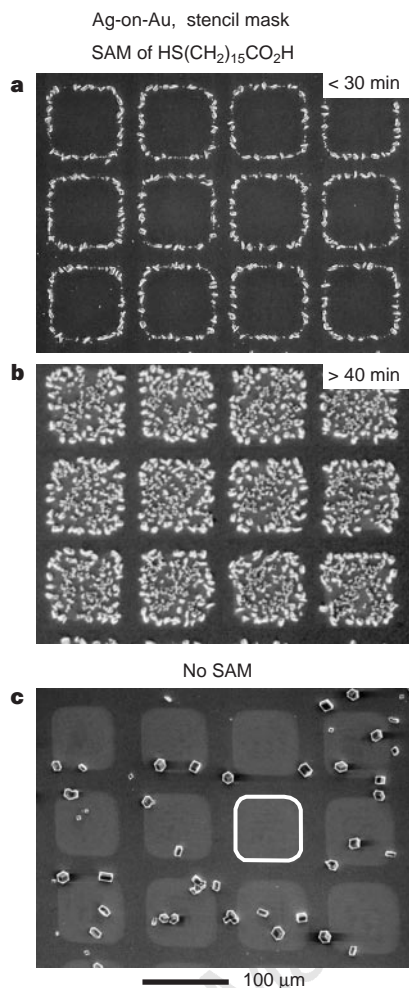


**Figure 3** Scanning electron micrographs of calcite crystals grown on topographically patterned surfaces fabricated by depositing Ag (50 nm) on Au through a stencil mask followed by formation of SAMs. The overlay shows the outline of the pattern. **a, b**, Patterns of calcite crystals formed on SAMs of HS(CH<sub>2</sub>)<sub>15</sub>CO<sub>2</sub>H supported on micropatterned metal surfaces. For short times of crystallization (<30 min), calcitic outlines of the underlying patterns are formed (**a**). For longer times of crystallization (>40 min), preferential filling of the Ag regions with crystals takes place (**b**). **c**, Non-patterned growth of calcite induced by bare substrates supporting no SAM. The patterned metal surfaces derivatized with a SAM of HS(CH<sub>2</sub>)<sub>15</sub>CO<sub>2</sub>H were used directly in the crystallization experiments (no exchange was performed). The substrates were placed with the pattern down into a 25 mM CaCl<sub>2</sub> solution in a closed desiccator containing vials of solid (NH<sub>4</sub>)<sub>2</sub>CO<sub>3</sub>.

Crystallization is highly sensitive to the structure and order of the surfaces that induce nucleation<sup>20–22</sup>. We used the formation of calcium carbonate as a model system<sup>22–24</sup>. The micropatterned Au-on-Ag and Ag-on-Au substrates supporting a CO<sub>2</sub>H-terminated SAM induce patterned crystallization (Fig. 3). The crystals nucleate first at the interface between the two metals (Fig. 3a), and then fill the Ag region (Fig. 3b). The bare, micropatterned metal surfaces (with no SAM) do not induce preferential nucleation anywhere on the surface (Fig. 3c); this observation indicates that patterned nucleation arises from differences in the structure of the patterned SAM and not directly from the topography of the surface. Figure 3 suggests that these techniques may provide a simple method to pattern crystal growth<sup>25</sup>. The fabrication of crystalline outlines (Fig. 3a) is especially striking, as these structures cannot be produced using other methods of crystallization.

The hypothesis that the transition regions in the SAMs are

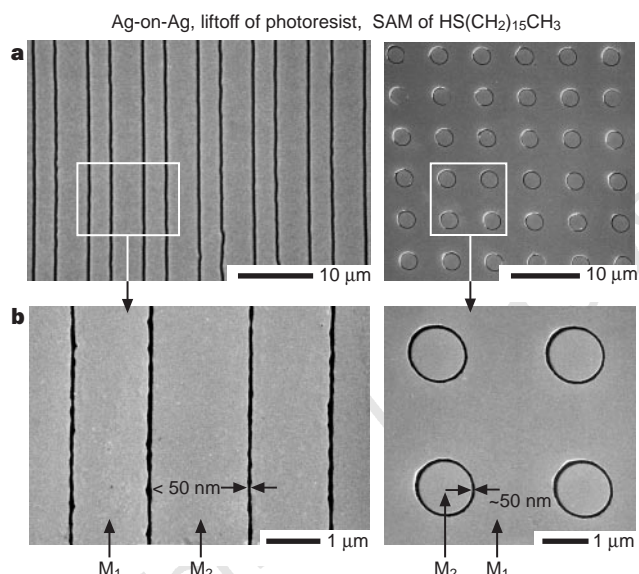


**Figure 4** Selective etching of micropatterned substrates fabricated by depositing Ag (50 nm) on a Ag film through a layer of patterned photoresist, followed by lift-off. Left panels, 2- $\mu$ m-wide lines; right panels, a square array of circles with 1.5  $\mu$ m diameter. **a**, Low magnification SEM, showing the homogeneity of the pattern. **b**, Trenches (~50 nm wide) in the metal substrates fabricated by etching for 10 s. Substrates were exposed to a HS(CH<sub>2</sub>)<sub>15</sub>CH<sub>3</sub> solution (10 mM in ethanol) for 1 h and rinsed with ethanol, then etched with an aqueous solution of ferrocyanide (0.1 M), ferricyanide (0.001 M) and sodium thiosulphate (0.1 M).

disordered suggests that these regions expose the underlying metal to etching<sup>15,26</sup>. When Ag-on-Ag or Au-on-Ag surfaces supporting a SAM of HS(CH<sub>2</sub>)<sub>15</sub>CH<sub>3</sub> were etched with an aqueous solution of potassium ferricyanide, dissolution of silver initiated preferentially at the border between the two metals (Fig. 4a). In control experiments with bare, topographically patterned substrates supporting no SAM, corrosion was uniform across the surface, and was not selective at the edges of the metal patterns. We suggest, again, that the specificity of etching at the transition regions results primarily from the disorder of the SAMs. The ability to etch the disordered regions in the SAM selectively provides a method to form small features in metal films<sup>1–3</sup>. The structures generated by etching topographically patterned surfaces supporting SAMs are smaller than the original patterns used for their generation, and their feature sizes can be controlled by varying the etching time. Figure 4b shows trenches ~50 nm wide in the metal substrates fabricated by short (10-s) etching, using two sample patterns of lines (Fig. 4b, left) and circles (Fig. 4b, right).

The ability to control the local disorder in SAMs at the nanometre scale therefore provides an approach to high-resolution patterning of surfaces, and constitutes a convenient method for size reduction: features less than 50 nm wide can be generated at the edges of micrometre-sized patterns. □

Received 17 April; accepted 9 June 1998.

- Moreau, W. M. *Semiconductor Lithography: Principles and Materials* (Plenum, New York, 1988).
- Smith, H. I. A Review of Submicron Lithography. *Superlat. Microstruct.* **2**, 129–133 (1986).
- Cerrina, F. & Marrian, C. A path to nanolithography. *MRS Bull.* **12**, 56–60 (1996).
- Kim, E., Xia, Y. & Whitesides, G. M. Polymer microstructures formed by moulding in capillaries. *Nature* **376**, 581–584 (1995).
- Berggren, K. K. *et al.* Microlithography by using neutral metastable atoms and self-assembled monolayers. *Science* **269**, 1255–1257 (1995).
- Chen, C. S., Mirksich, M., Huang, S., Whitesides, G. M. & Ingber, D. E. Geometric control of cell life and death. *Science* **276**, 1425–1428 (1997).
- Bunker, B. C. *et al.* Ceramic thin-film formation on functionalized interfaces through biomimetic processing. *Science* **264**, 48–55 (1994).
- Hu, J. *et al.* Using soft lithography to fabricate GaAs/AlGaAs heterostructure field effect transistors. *Appl. Phys. Lett.* **71**, 2020–2022 (1997).
- Ulman, A. *Introduction to Thin Organic Films: From Langmuir-Blodgett to Self-Assembly* (Academic, Boston, 1991).

10. Nuzzo, R. G., Dubois, L. H. & Allara, D. L. Fundamental studies of microscopic wetting on organic surfaces. 1. Formation and structural characterization of a self-consistent series of polyfunctional organic monolayers. *J. Am. Chem. Soc.* **112**, 558–569 (1990).
11. Laibinis, P. E. *et al.* A comparison of the structures and wetting properties of self-assembled monolayers of *n*-alkanethiols on the coinage metal surfaces Cu, Ag, Au. *J. Am. Chem. Soc.* **113**, 7152–7167 (1991).
12. Dulcey, C. S. *et al.* Deep UV photochemistry of chemisorbed monolayers: patterned coplanar molecular assemblies. *Science* **252**, 551–554 (1991).
13. Tiberio, R. C. *et al.* Self-assembled monolayer electron beam resist on GaAs. *Appl. Phys. Lett.* **62**, 476–478 (1993).
14. Kumar, A., Abbott, N. A., Kim, E., Biebuyck, H. A. & Whitesides, G. M. Patterned self-assembled monolayers and meso-scale phenomena. *Acc. Chem. Res.* **28**, 219–226 (1995).
15. Xia, Y., Zhao, X. M. & Whitesides, G. M. Pattern transfer: self-assembled monolayers as ultrathin resists. *Microelectr. Eng.* **32**, 255–268 (1996).
16. Larsen, N. B., Biebuyck, H., Delamarche, E. & Michel, B. Order in microcontact printed self-assembled monolayers. *J. Am. Chem. Soc.* **119**, 3017–3026 (1997).
17. Abbott, N. L., Folkers, J. P. & Whitesides, G. M. Manipulation of the wettability of surfaces on the 0.1- to 1-micrometer scale through micromachining and molecular self-assembly. *Science* **257**, 1380–1382 (1992).
18. López, G. P., Biebuyck, H. A., Frisbie, C. D. & Whitesides, G. M. Imaging of features on surfaces by condensation figures. *Science* **260**, 647–649 (1993).
19. Kumar, A. & Whitesides, G. M. Patterned condensation figures as optical diffraction gratings. *Science* **263**, 60–62 (1994).
20. Landau, E. M., Levanon, M., Leiserowitz, L., Lahav, M. & Sagiv, J. Transfer of structural information from Langmuir monolayers to three-dimensional growing crystals. *Nature* **318**, 353–356 (1985).
21. Stupp, S. I. & Braun, P. V. Molecular manipulation of microstructures: biomaterials, ceramics, and semiconductors. *Science* **277**, 1242–1248 (1997).
22. Heywood, B. R. & Mann, S. Template-directed nucleation and growth of inorganic materials. *Adv. Mater.* **6**, 9–20 (1994).
23. Berman, A. *et al.* Total alignment of calcite at acidic polydiacetylene films: cooperativity at the organic-inorganic interface. *Science* **269**, 515–518 (1995).
24. Weiner, S. & Addadi, L. Design strategies in mineralized biological materials. *J. Mater. Chem.* **7**, 689–702 (1997).
25. Mann, S. & Ozin, G. A. Synthesis of inorganic materials with complex form. *Nature* **382**, 313–318 (1996).
26. Zhao, X.-M., Wilbur, J. L. & Whitesides, G. M. Using two-stage chemical amplification to determine the density of defects in self-assembled monolayers of alkanethiolates on gold. *Langmuir* **12**, 3257–3264 (1996).

**Acknowledgements.** This work was supported in part by the ONR and DARPA. It used MRSEC Shared Facilities supported by the NSF.

Correspondence and requests for materials should be addressed to G.M.W. (e-mail: gwwhitesides@gmwgroup.harvard.edu).

## Decadal variability in the outflow from the Nordic seas to the deep Atlantic Ocean

Sheldon Bacon

Room 256/43, Southampton Oceanography Centre, Empress Dock, Southampton SO14 3ZH, UK

The global thermohaline circulation is the oceanic overturning mode, which is manifested in the North Atlantic Ocean as northward-flowing surface waters which sink in the Nordic (Greenland, Iceland and Norwegian) seas and return southwards—after overflowing the Greenland–Scotland ridge—as deep water. This process has been termed the ‘conveyor belt’, and is believed to keep Europe 5–8 °C warmer than it would be if the conveyor were to shut down<sup>1</sup>. The variability of today’s conveyor belt is therefore an important component of climate regulation. The Nordic seas are the only Northern Hemisphere source of deep water and a previous study<sup>3</sup> has revealed no long-term variability in the outflow of deep water from the Nordic seas to the Atlantic Ocean. Here I use flows derived from hydrographic data to show that this outflow has approximately doubled, and then returned to previous values, over the past four decades. I present evidence which suggests that this variability is forced by variability in polar air temperature, which in turn may be connected to the recently reported Arctic warming<sup>4</sup>.

The water which overflows the shallow (500–700 m) Greenland–Scotland ridge east and west of Iceland descends to depths around 3,000 m in the northern North Atlantic, and follows paths which are well known<sup>5–7</sup>, but the prevailing view of the temporal variability of

the magnitude of the flow has been that it possesses no significant variability on timescales longer than about a fortnight<sup>3</sup>. The Nordic seas and the Arctic have been seen as a black box or reservoir whose exchanges with the rest of the world ocean are governed solely by hydraulics because shallow convective processes keep the waters at the sill depth ‘topped up’. Following the evidence presented below, it appears that shallow processes are responsive to atmospheric forcing in such a way that the Nordic seas exert important control on the variability of the conveyor belt.

Water from the Nordic seas which overflows the Greenland–Scotland ridge east of Iceland travels round the Mid-Atlantic Ridge (MAR) by way of the Charlie–Gibbs fracture zone; in the northwest of the Irminger basin, it joins the water which overflows west of Iceland through Denmark Strait. South of Denmark Strait, these waters form the Deep Western Boundary Current (DWBC), which has characteristic chemical and dynamical signatures<sup>5–7</sup>. In particular, the vertical current shear near the bottom is very high, so a large part of the flow can be measured with the shear derived from hydrographic data. Without knowledge of the absolute current, one can create a 40-year history of the DWBC from archive data by using the transport referenced to a constant zero-velocity surface as an index of the strength of the DWBC.

I have analysed 22 sections, the earliest from 1955, the most recent from August 1997 (Fig. 1). They lie in the vicinity of Cape Farewell, and radiate between southwards (at ~43° W) and eastwards (at ~60° N) from Cape Farewell across the Irminger Sea. The core of the DWBC spans ~200 km of downstream distance over the sections, with the exception of the section at 62° N which was included to fill an important time gap. Being further north than the rest, the flux estimate from there may not be quite consistent with the others. The sections are far enough downstream from Denmark Strait that the DWBC is flowing nearly parallel to the isobaths and not significantly changing strength by entrainment over much of the span of the sections<sup>8</sup>, with the possible exception of the 62° N section. The DWBC volume flux is consistently and correctly estimated in spite of differently angled tracks of the sections across the current, assuming no significant deep flow normal to the central axis of the basin<sup>8,9</sup>.

Calculating (as previous authors have done) the DWBC as transport below the density surface  $\sigma_0 = 27.8$ , with zero velocity at 1,000 m, a picture of DWBC magnitude and variability emerges (Fig. 2). Low transports (nine estimates) appear in the 1950s and 1960s, high (four estimates) in the 1970s and 1980s, and low again (nine estimates) in the 1990s. Is this noise or a signal? First, there is no bias with section orientation or season. Second, were it true for the present data set as for previous ones that the dominant variability period is a few days, this set would be the product of a random process. This hypothesis may be tested by dividing the data into three groups as above and comparing the first with the second and the second with the third (using a non-parametric ranking or mean slippage test such as Wilcoxon’s<sup>10</sup>). In both cases, the chance that the pattern is random is <0.5%.

The relative invariance of the referenced transport signal on short time and space scales is tested by examining two groups of sections: four sections taken over four weeks in spring 1966, and five sections taken over five months around summer 1991 (Fig. 1, left and right insets). These two groups have mean transports (standard errors in parentheses) of 5.8 (0.2) Sv (first group; 1966), and 4.5 (0.2) Sv (second group; 1991) (1 Sv = 10<sup>6</sup> m<sup>3</sup> s<sup>-1</sup>). The ‘short-scale’ range (0.2 Sv) is an order of magnitude less than the decadal range. Therefore I treat the pattern as a signal.

What of the transport due to the reference level current? First, recent modelling studies<sup>11,12</sup> indicate that the Irminger basin circulation is not strongly dependent on variations in the wind stress. The referenced transport signal is unlikely to have been altered by the wind-driven circulation in such a way as to annul exactly the observed variability. Second, absolute transports are available in two